ORIGINAL PAPER

Evaluation of a Refined Implantable Resonator for Deep-Tissue EPR Oximetry in the Clinic

**Eunice Y. Chen[1,2] · Dan Tse[2,3] · Huagang Hou[2,3] · Wilson A. Schreiber[2,3] ·
Philip E. Schaner[2,4] · Maciej M. Kmiec[2,3] · Kendra A. Hebert[2,3] ·
Periannan Kuppusamy[2,3] · Harold M. Swartz[2,3,4] · Benjamin B. Williams[2,3,4]**

© The Author(s), under exclusive licence to Springer-Verlag GmbH Austria, part of Springer Nature 2021

Abstract

(1) Summarize revisions made to the implantable resonator (IR) design and results of testing to characterize biocompatibility; (2) Demonstrate safety of implantation and feasibility of deep tissue oxygenation measurement using electron paramagnetic resonance (EPR) oximetry. In vitro testing of the revised IR and in vivo implantation in rabbit brain and leg tissues. Revised IRs were fabricated with 1–4 OxyChips with a thin wire encapsulated with two biocompatible coatings. Biocompatibility and chemical characterization tests were performed. Rabbits were implanted with either an IR with 2 oxygen sensors or a biocompatible-control sample in both the brain and hind leg. The rabbits were implanted with IRs using a catheter-based, minimally invasive surgical procedure. EPR oximetry was performed for rabbits with IRs. Cohorts of rabbits were euthanized and tissues were obtained at 1 week, 3 months, and 9 months after implantation and examined for tissue reaction. Biocompatibility and toxicity testing of the revised IRs demonstrated no abnormal reactions. EPR oximetry from brain and leg tissues were successfully executed. Blood work and histopathological evaluations showed no significant difference between the IR and control groups. IRs were functional for up to 9 months after implantation and provided deep tissue oxygen measurements using EPR oximetry. Tissues surrounding the IRs showed no more tissue reaction than tissues surrounding the control samples. This pre-clinical study demonstrates that the IRs can be safely implanted in brain and leg tissues and that repeated, non-invasive, deep-tissue oxygen measurements can be obtained using in vivo EPR oximetry.

✉ Benjamin B. Williams
   Benjamin.B.Williams@hitchcock.org

Extended author information available on the last page of the article

1 Introduction

Tumor hypoxia is known to impart resistance to radiation therapy and chemotherapy [1–4] and to portend poorer prognoses and outcomes regardless of treatment modality as a result of hypoxic cells having accelerated malignant progression and increased metastatic potential [5–9]. Various methods have been used to determine oxygen status in solid tumors in attempts to investigate and develop hypoxia-modifying approaches to target hypoxic cells to improve treatment efficacy [10–13]. 18-F Fluoro-misonidazole positron emission tomography (FMISO PET), blood/tumor oxygen level dependent magnetic resonance imaging (BOLD/TOLD MRI), and dynamic contrast enhancing (DCE) MRI are non-invasive imaging modalities which have been used both preclinically and clinically to provide information about tumor oxygen before and during treatments [14–17]. Eppendorf oxygen-sensitive electrodes have been used clinically to provide an assessment of oxygen levels; however, this technology is invasive and no longer available [5, 18–20].

In vivo electron paramagnetic resonance (EPR) oximetry utilizing a variety of oxygen probes (e.g. India ink, carbon char, lithium phthalocyanine, OxyChip, and implantable resonator) has been shown in animal and preclinical studies [21–25] as well as human clinical trials [26–28] to be a valuable tool to assess tumor and tissue oxygenation repeatably and reliably. The first-in-human clinical trial with 24 patients showed that EPR oximetry with the paramagnetic oxygen probe, OxyChip, was safe and feasible [27]. The OxyChip is composed of lithium octa-*n*-butoxynaphthalocyanine (LiNc-BuO) crystals embedded in polydimethylsiloxane (PDMS) [29–31]. This trial highlighted a number of potential improvements to EPR oximetry to make this technology more versatile and useful to most, if not all, solid tumors. However, with the technologies used, specifically OxyChip probes detected using surface-loop resonators at L-band (1.15 GHz), limited radiofrequency (RF) penetration prevents detection of the signal from probes implanted at a depth of more than a centimeter or two from the skin [32]. Efforts to extend the range of depth in tissues accessible for in vivo EPR measurements have included exploration of the use of lower frequencies with greater RF penetration [33–35], improvements in detection sensitivity via pulsed acquisition [36–38], and the design of novel resonator detector systems [39, 40].

Over the last 30 years, implantable resonator (IR) systems have been developed that enable EPR measurements to be performed with paramagnetic probes located in tissues at depths of at least 20 cm [41–49]. Initially developed for use in animals, the implantable resonators have been revised and improved, and are approaching readiness for use in human subjects. The studies described in this manuscript are intended to support clinical translation and regulatory approval to enable their use in human subjects. The implantable resonator systems are comprised of an EPR spectrometer with external surface loop resonator [39] that is inductively coupled to an implanted structure containing conductive wire and oximetric paramagnetic material. For simplicity, the implanted structure will be referred to as the implantable resonator. The wire is formed into a coupling loop
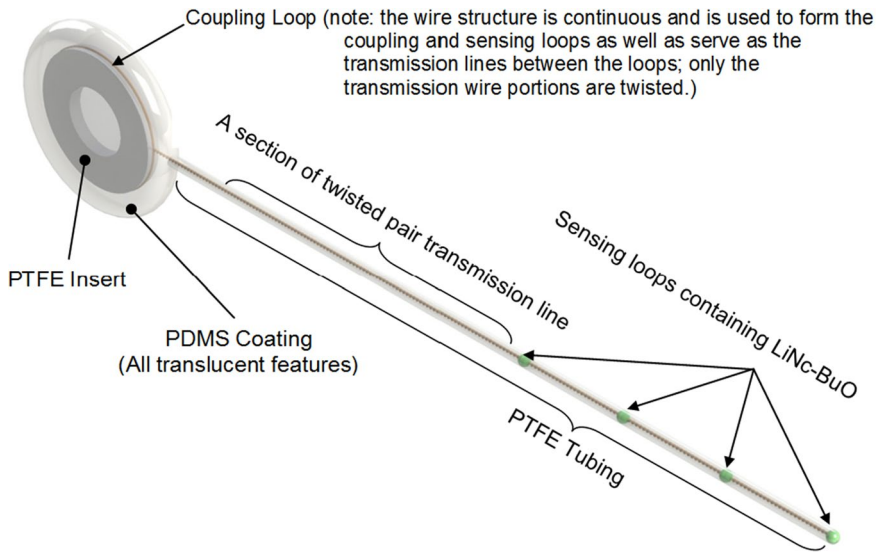
Fig. 1 Drawing of the IR for human use, showing the names of the features. Note: the coupling loop, when implanted, will be placed below the skin with the flexible transmission line and sensors at an angle to the skin surface (not linear as displayed)

Fig. 2 Photographs of two different length IRs. (Top) An IR with a 50-mm transmission line and 4 sensors. (Bottom) An IR with an 18-mm transmission line and 2 sensors
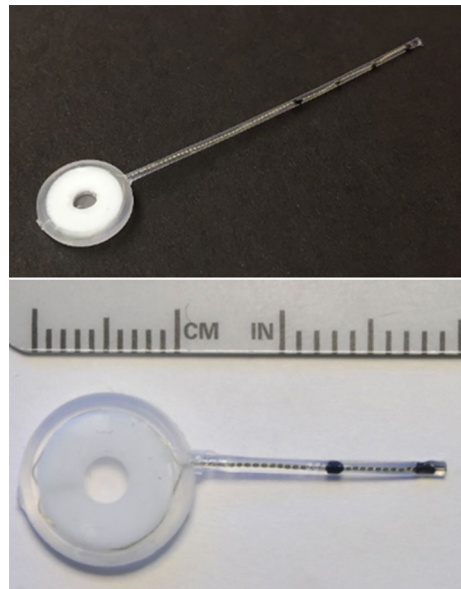
and one or more small sensor loops containing paramagnetic material that are all connected via sections of twisted pair transmission lines (Figs. 1, 2). A single wire is used to form the conductive structure of the IR, with the ends meeting and left disconnected at the edge of the coupling loop. With this design, when

coupled with the external surface loop resonator, the resonance frequency of the system is dominated and determined by the external resonator. This strategy allows implanted structures of varying lengths to be coupled with the same external loop resonator tuned to 1.15 GHz and used at the fixed magnetic field strength of our clinical electromagnet (410 G). The implanted coupling loop remains close to the surface and the sensor loops are positioned within the tissue of interest. The RF energy for EPR detection is inductively injected into the IR and propagated directly via the transmission line sections to the paramagnetic sensors without losses associated with travel through lossy tissue.

Prior developments of the IR system reported by Caston et al. [42] helped to advance its translation into clinical practice through the incorporation of biocompatible MP35N wire (California Fine Wire Products Corp., Grover Beach, CA), PDMS coating materials, and LiNc-BuO as the oxygen-sensing probe. For IR fabrication, LiNc-BuO crystals were synthesized, crushed, and placed in a PDMS polymer via the methods described in [29–31]. As detailed in the supplementary IR manufacturing steps, the uncured LiNc-BuO/PDMS is inserted into each individual sensing loop using a dispensing needle in such a manner that fully encapsulates each sensing loop and is then cured. The sensing loop, containing LiNc-BuO, is nominally 0.7 mm in diameter; however, the size of the sensing loops can vary due to the nature of our current manufacturing methods. After the observation of an unacceptably high frequency of breakage when copper was used, MP35N wire was chosen for subsequent use, due to its high tensile strength, established biocompatibility, and more than adequate signal-to-noise ratio (SNR) under practical conditions (see Fig. 6). Consideration of manufacturing details and procedures for use, as well as requirements for formal biocompatibility and safety were described previously [42]. Formal MRI safety testing was performed according to American Society for Testing and Materials (ASTM) standards to evaluate displacement forces, torque, artifact generation, and heating. It was determined that the IR is 'MRI Conditional', and that a patient with this device can safely be scanned in an MR system with static field of 1.5 T or 3 T, maximum spatial gradient of 40.0 T/m, and maximum MR system reported specific absorption rate (SAR) of 2 W/kg. Initial results of tests with the implantable resonator system in animal models revealed needs for modifications to enhance mechanical robustness, to facilitate the implantation procedure, to reduce tissue adherence to the resonator surface, to ensure more reliable containment of the paramagnetic material, and to standardize the fabrication process. In this paper, we describe the refinements to the implantable resonator design, the results of the biocompatibility testing, and the preclinical study in which the refined implantable resonators were placed in the brain and leg of rabbits and oxygen measurements by EPR were made.

2 Materials and Methods

2.1 Implantable Resonator Design Revisions

A design variant of the implantable resonator with a very thin outer polytetrafluoroethylene (PTFE) layer surrounding the transmission line and sensor loops was developed to secure the OxyChip probes from dislodgement and to minimize

tissue adherence. This layer was formed of PTFE tubing (PTFE Sub-Lite-wall tubing (Extruded) with an inside diameter of 1.02 mm (0.0400 inch) and wall thickness of 0.038 mm (0.0015 inch) (Zeus Medical, Orangeburg, SC). This design refinement provides increased mechanical strength and a smoother, less tacky surface for implantation via a catheter and subsequent removal from the tissue. Despite this minimal thickness of the PTFE, there was concern that it might transmit oxygen longitudinally and thereby affect the ability of neighboring sensors to independently equilibrate with the surrounding tissue. Measurements were performed using a custom-built equilibration chamber, similar to that used in [42], where neighboring sensors could be exposed to different pO$_2$ levels and the independence of their readouts could be assessed. It was observed that the sensors, separated by 7 mm, did respond independently from each other, with a response time for equilibration to their environments of approximately $t_{1/2} = 90$ s. This study supported the utility of the revised IR design for multi-site pO$_2$ measurements and enabled the minimally invasive implantation procedure described below. An additional modification to the implantable resonator was the placement of a permanent PTFE washer in the coupling loop to keep its circular shape and to provide a more readily palpable feature of the implantable resonator to help with localization during measurements.

The implantable resonator was initially designed to be deployed via passage through a narrow gauge needle (ca. 18G) that was inserted into the tissue with its tip in the tissue of interest [42], similar in practice to the implantation of brachytherapy seeds for radiation therapy and the implantation procedure for the OxyChip [27]. Following insertion of the needle, the implantable resonator would be placed in lumen of the needle, and the needle would then be removed leaving the resonator in place with the sensor loops in the tissue of interest. Following removal of the needle, the collapsed coupling loop would then need to be reshaped to the original form and stabilized with a circular PTFE disc insert. While this approach was feasible, it proved to be challenging due to tackiness of the surfaces of the implantable resonator and the need to reform the shape of the coupling loop. A commercial peel-away catheter (Adelante SafeSheath UltraLite, Oscor #ASUP051318P) was identified to replace the needle for targeted introduction of the resonator into the tissue of interest. The peel-away catheter is split into two pieces during its removal from the tissue, alleviating the need for passage of the coupling loop through the lumen, and thus allowing the whole implantable resonator to be performed and hold its shape throughout the deployment process (Fig. 3). Figure 1 and illustrate the finalized IR design for human use. The length of the transmission line and number of sensors can be adjusted, but the fabrication steps as detailed in supplemental materials are otherwise identical.

2.2 Biocompatibility Testing

The biocompatibility of the implantable resonator was formally evaluated in a series of tests carried out according to ISO 10993 guidelines via contract with an external GLP-accredited laboratory (Pacific Biolabs, Hercules, CA). The testing included Cytotoxicity (ISO 10993–5), Sensitization (ISO 10993–10), Reactivity

Fig. 3 IR implantation using a peel-away catheter

(ISO 10993–10), Endotoxin (USP < 85>), and Pyrogenicity (ISO 10993–11). For chemical characterization, liquid and gas chromatography-mass spectrometry (LC/GC–MS) for organic extracts, inductively coupled plasma-mass spectrometry (ICP-MS) for inorganics and heavy metals extracts, and Fourier transform infrared spectroscopy (FTIR) were performed.

2.3 Rabbit Implantation Study

All procedure were reviewed and approved by the institutional animal care and use committee (IACUC). Twenty-four New Zealand white rabbits (Charles River Laboratories, Wilmington, MA), 2–4 kg, 22–24 weeks, arrived in three separate shipments for three cohorts (1 week, 3 months and 9 months, each 8 rabbits). All animals appeared clinically healthy on arrival. They were housed following standard procedures.

2.4 Implantation of IRs into Brain and Hind Leg Soft Tissue

The procedure for implantation of an IR was similar to that for other implanted EPR oximetry probes [23], but a peel-away catheter was introduced to facilitate implantation of the coupling loop of the IR that did not fit through the bore of a conventional needle or catheter. IRs were fabricated as described in the supplement and sterilized via steam sterilization in the autoclave at gravity cycle (at 121 °C and 15 PSIG for 30 min). The procedure used for this rabbit study was similar to that envisioned for clinical use.

Rabbits were sedated in the veterinary operating room, anesthetized with 3% isoflurane in 30% O_2 and maintained using 2.5% isoflurane with 30% O_2. Lidocaine was applied at the surgical site. Analgesia (Ketoprofen 3 mg/kg and Buprenorphine 0.02–0.05 mg/kg) were administered immediately before and again within the first 48 h after implantation surgery. Blood was collected for complete blood count

(CBC) and a comprehensive metabolic profile (CMP). Physiological parameters (respiratory rate, behavior, body condition score and body weight) were monitored periodically and recorded.

For the implantation of IRs into the brain tissue, the head was shaved, cleaned and antiseptically treated with Betadine, and then 70% alcohol scrubs for three times. A small incision (2–3 cm) was made on the skin. After careful separation of the connective tissue and exposure of the skull, a 2–5 mm craniotomy was made with a drill on the right skull at predefined co-ordinates [AP (anterior–posterior from bregma): − 3.5 mm; ML (medial-right lateral from midline): 4 mm on right hemisphere]. These co-ordinates were based on the published reports and our experiences in previous studies [22, 50]. The dura was gently opened with a 14–18G needle. For each rabbit, we used an 8 mm length IR with two sensory probes (similar to Fig. 2) and the coupling loop connected together with transmission line in a single unit that can be lowered to the target area of the brain at once without the need to use angiocatheters to guide insertion of the IR. Figure 2 shows the IR as used for these rabbit studies with two sensory loops. The coupling loop of the IR was placed over the skull. Figure 4 shows the location of the sensor loops in the brain and the coupling loop on the surface of the skull (under the skin). The incision on the skin was closed with non-absorbable 3–0 nylon suture. For the control group of animals, a rod of biocompatible material (high-density polyethylene-(HDPE)) of similar dimensions and flexibility as the IR was inserted in a manner similar to that described for the IR above.

For implantation of the IR into the leg, the procedure envisioned for clinical use with peel-away catheter was used. The right hind leg was shaved, cleaned and scrubbed with Betadine and 70% alcohol alternating three times. IRs with two sensor loops were used, identical to those used in the brain. A small incision
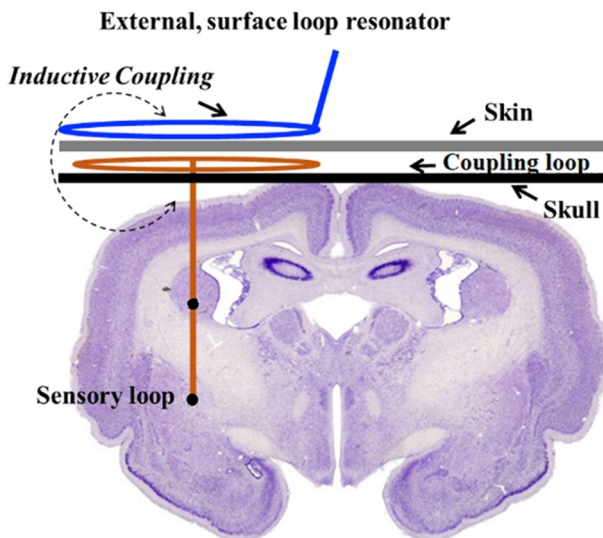

Fig. 4 Anatomy of the rabbit brain showing the location of sensory loop, transmission line and coupling loop of IR in the brain

(1–2 cm) was made on the skin and a small subcutaneous pocket was created to later place the coupling loop. An 18G brachytherapy needle was inserted through the incision into the hind leg soft tissue aiming for the biceps femoris or vastus lateralis muscle. The brachytherapy stylet was removed. A sterile guide wire was inserted through the needle and the needle was removed leaving the wire in place. Next the peel away catheter with introducer was passed over the wire and tunneled into the soft tissue. Once the peel away catheter/introducer was inserted at the appropriate depth, the sterile wire and introducer were removed with the peelaway catheter left in place. The IR was then passed through the catheter to the desired depth and the peel-away catheter was removed leaving the IR in place in the soft tissue (Fig. 3). The coupling loop was buried under the skin and secured with a single simple absorbable suture at its junction with the transmission line. The incision on the skin was closed with absorbable suture. For the control group of animals, a rod of biocompatible material (high-density polyethylene-HDPE) of similar dimensions as the IR was inserted in the right hind leg in a manner similar to that described for the IR above. The rabbits were observed every 2 h during the first 6 h after the implantation, followed by daily observation for first week, and then weekly observation for the remainder of the study.

2.5 EPR Oxygen Measurements

All oximetry measurements were performed using a clinical EPR spectrometer with an external surface-loop resonator operating at L-Band (1.15 GHz) [51]. An electromagnet with 3D gradients for spatial localization of signals from IRs with multiple sensor loops was used. Prior to implantation, measurements under N_2 conditions were performed for all IRs to verify basic functionality. Oxygen calibration was performed for a representative set of resonators ($N = 4$).

For repeated measurements of pO_2 in the EPR lab (excluding the day of surgery), the rabbits were placed in an induction box, 2.0–2.5% isoflurane in 30% O_2 was perfused for 15–20 min, and then the isoflurane was increased to 2.5–3.5% for another 10–15 min to completely anesthetize the rabbits. During anesthesia, the rectal temperature of the rabbits was monitored using a rectal probe and maintained within a normal range (38.3–39.4 °C) using a warm water pad and/or warm air. Blood oxygen saturation ($SpaO_2$) and heart rate were also monitored using a pulse oximeter clamped to the ear or toe. The rabbits were transferred to the EPR spectrometer on a plate fitted with a nose cone and 2.5–3.0% isoflurane was continued. The rabbits were placed between the magnet poles of the EPR spectrometer and an external surface loop resonator was gently placed on the head or leg, in close proximity to the implanted coupling loop, and pO_2 measurements were performed. The animals with IRs underwent measurements of oxygen performed 2 or 3 times each during the course of the experimental protocol. Following explantation of the implanted resonators, oxygen calibration was performed for comparison with pre-implantation measurements.

2.6 Euthanasia and Gross Pathology

Animals to be euthanized were anesthetized with isoflurane. A blood sample for CBC and biochemical analysis was obtained from an ear vein prior to administration of heparin to improve perfusion. Following euthanasia (pentobarbital given IV into an ear vein), the thoracic cavity was opened and organs perfused via the left ventricle using 0.9% saline to clear the tissues of blood followed by 10% formalin for fixation.

Gross necropsy included observation of organs including examination of the location of the coupling loop and transmission line and the surrounded tissues. The implant was either removed (IR) or left in the tissue (HDPE) to facilitate dissection. Whole brain, hind leg muscle surrounding the device, sections of liver, kidneys, lymph nodes, spinal cord, heart, lungs, stomach, and intestines were removed and stored in 10% formalin for later histological analysis.

2.7 Histopathology

Hematoxylin and eosin (H+E) was used to stain sections of the skeletal muscle tissue from rabbits. Tissues were obtained from non-implanted rabbits as well as IR implanted rabbits after 9 months. At the end of the experiments, the rabbits were euthanized and the tissue containing IRs and control implants were excised and fixed in 10% formalin. The IRs were removed from the muscle and were recalibrated. Tissues were embedded in paraffin and stained with hematoxylin+eosin for histological studies.

3 Results

3.1 Final Design of Implantable Resonator with PDMS/HDPE Coating and 2 Sensor Loops

Fabrication of IRs with the described design revisions was successful. Details regarding the materials and procedures used for fabrication the implantable resonators are provided as a supplement. Quality assurance steps included visual inspection of the IRs to verify that the biocompatible PDMS coatings were complete, confirmation that the OxyChip material had been properly localized in each of the sensor loops, batch oximetric calibration, and basic functionality testing. Gross manufacturing failures and close visual inspections eliminated approximately 10% of resonators, with the most common deficiencies related to PDMS molding errors. Excluding resonators with apparent manufacturing defects, all remaining resonators passed basic functionality testing, with the expected pair of EPR signals measured from the two sensing loops under nitrogen equilibration and static gradient acquisition conditions. Calibration of a subset of resonators ($N=4$) under N_2, 2% O_2, and 5% O_2 provided oximetric sensitivity of 10 ± 1 mG/mmHg with an anoxic linewidth of 108 ± 5 mG.

3.2 Biocompatibility Testing

The biocompatibility and chemical characterization of the implantable resonator, as the test article, was evaluated in a series of tests carried out according to ISO 10993 guidelines via contract with an external GLP-accredited laboratory (Pacific Biolabs, Hercules, CA).

Cytotoxicity (ISO 10993-5): cells treated with the test article extract exhibited a response of grade 0 (no reactivity) at 24 and 48 h. Based on qualitative evaluation of the cells exposed to the test article extract, the test article was not considered to have a cytotoxic effect.

Sensitization (ISO 10993-10): no sensitization reactions or patterns were noted in tested guinea pigs exposed to test article extracted in either saline or cottonseed oil. The test animals did not receive scores higher than those of the negative control animals. The test article when extracted in saline or cottonseed oil, did not elicit sensitization reactions in animals used in this study.

Reactivity (ISO 10993-10): based on erythema and edema scores, the test article extracted in saline or cottonseed oil did not elicit biologically significant irritation reactions when compared to the control after being injected intracutaneously in rabbits. The test article extracted in saline or cottonseed oil met the requirements for the Intracutaneous (Intradermal) Reactivity Test.

Endotoxin (USP <85>): the results of the positive product control were within 50–200% of the known spike endotoxin concentration when tested at the following dilutions: undiluted, 1:10, 1:20, 1:40 and 1:80. Two additional lots for validation are needed to complete the recommended three lot validation for this product. The test article passed the validation (Inhibition/Enhancement) test based on the USP and ANSI/AAMI ST72 specified acceptance criteria for this test.

Pyrogenicity (ISO 10993-11): all rabbits appeared healthy during the test and none exhibited an individual increase in temperature of 0.5 °C or more when compared to the control temperature. Based on criteria for this test, the test article met the USP <151> requirements for the absence of pyrogens.

3.3 Chemical Characterization

Gas chromatography-mass spectrometry (GC–MS) was performed to assess volatile and semi-volatile organic extracts. Water extract exhibited one unique peak above the 1 ppm internal standard when compared to the corresponding blank extract, with potential identification as acetamide. Ethanol extract exhibited 23 unique peaks above the 1 ppm internal standard when compared to the corresponding blank extract. All peaks were tentatively identified as various forms of siloxanes.

Liquid chromatography–mass spectrometry (LC–MS) was used to identify the presence of larger molecular weight and non-volatile compounds. Water extract exhibited two unique peaks above the 1ppm internal standard, with one conforming to the acetamide peak observed with GC–MS and the other indicative of a siloxane compound. Ethanol extract exhibited 34 peaks, mostly identified as siloxanes, above

the 1-ppm standard. Non-siloxane molecules in positive mode extracts included $C_{10}H_{13}NO_2$ and $C_{32}H_{44}O_2$. Negative mode extracts tentatively identified 2,6-di-tert-butyl-4-(4-hydroxybenzyl)phenol or isomer ($C_{23}H_{48}O$) and 4-({4-[4-(2-methyl-2-propanyl)phenoxy]phenyl}amino)-4-oxobutanoic acid ($C_{20}H_{23}NO_4$).

Inductively coupled plasma-mass spectrometry (ICP-MS) for inorganics and heavy metals extracts was performed. Copper and antimony were detected in the water extract of the device above the limit of quantitation. Antimony was recovered at 0.001477 µg/device and copper was recovered at 0.002526 µg/device.

Fourier transform infrared spectroscopy (FTIR) showed no significant difference between the sample extract and the blank water extract. Similarly, the ethanol extract showed no significant difference between the sample extract and the blank ethanol extract.

3.4 In vivo Rabbit Study

In this study, 24 New Zealand white rabbits were implanted with either implantable resonators or HDPE control material in the brain and in the hind flank. This study was designed to test the feasibility of pO_2 measurement and evaluation of histological changes after short term and long term implantation in the brain and soft tissue of rabbits. Over the course of the study, we monitored the neurobehavioral and systematic toxicity in awake animals including observing respiratory rate, motor activities, convulsion, reflexes, and body weight, and measured pO_2 in anesthetized rabbits. Figure 5 shows rabbit body weights recorded for the 9-month cohort; weights for other cohorts were consistent. At 3 specific end points (1-week, 3-month and 9-month post-implantation) cohorts of 8 rabbits were anesthetized, blood analyses performed, and tissues collected for pathology.
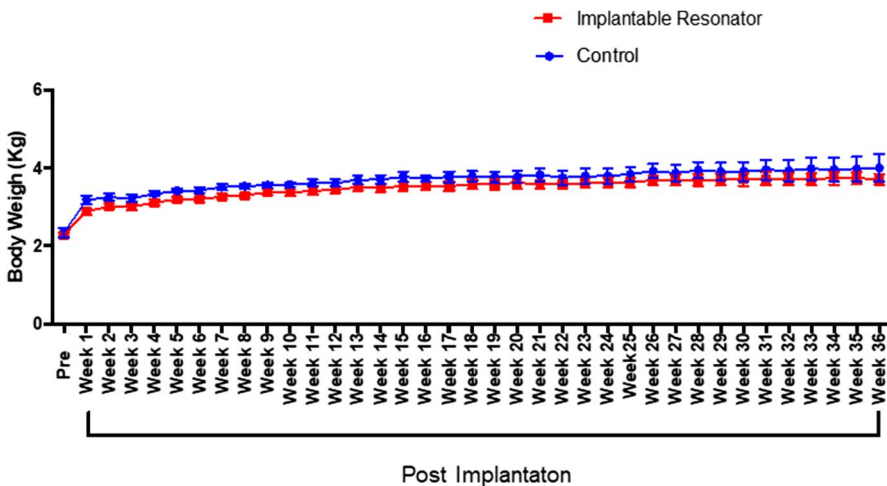

Fig. 5 Rabbit body weight measured over 9 months. No difference in weight between those rabbits implanted with IR vs Control

3.5 Rabbit Implantations, Surgery and Postoperative Status

The IR implantation procedure itself was uneventful in 11 of 12 rabbits. One rabbit had to be euthanized due to unexpected neurological complications related to self-inflicted displacement of the IR resulting in tissue damage and hemorrhage under the incision. For the 12 rabbits implanted with negative control HDPE samples, three had to euthanized, including one experiencing persistent leg pain and two related to unexpected brain injuries.

For the 1-week and 3-month cohorts, all IRs were explanted intact without evidence of damage or breakdown incurred during residence in the animals. In the 9-month cohort, a single IR in the leg of one rabbit was observed during the course of the study to contain a fractured wire at the junction between the transmission line and the coupling loop. The remaining resonators in the 9-month cohort showed no evidence of damage prior to removal, though one of the resonators from a hind leg was observed to have a broken wire upon inspection after explantation. This resonator was fully functional 1-week earlier in vivo, and it is assumed that it was damaged during the removal procedure.

3.6 Rabbit Oxygen Measurements

In vivo measurements of oxygen were performed for the rabbits in the 3-month and 9-month cohorts (e.g. Fig. 6). For the intracranial sites, the measurements were consistent across time and animals, though with a statistically significant difference in the pO_2 between the deep and more shallow sites (41 ± 6 mmHg vs 47 ± 6, $p < 0.01$, $N = 22$ each). Measurements from the hind leg were more variable, (25 ± 15 mmHg, $N = 38$), with no detectable difference between the two sensors for each IR. Data for each measurement are included in Table 1. Intra-cranial measurements are consistent with prior deep brain tissue measurement made with a different implantable resonator design [22]. Similarly, hind leg measurements are consistent with earlier measurements made in rabbits using EPR with EMS char [52].
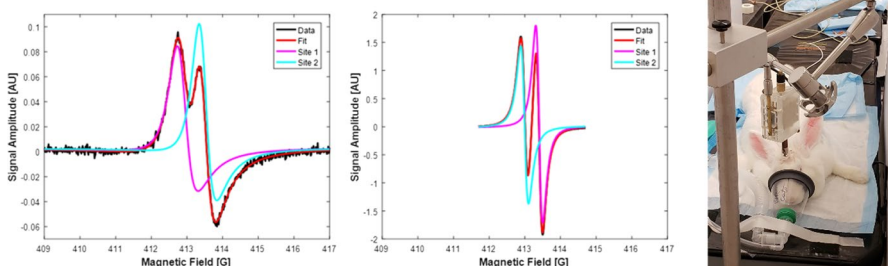

Fig. 6 Representative EPR spectra measured from IRs in the brain (left) and leg (center). A rabbit positioned for brain pO_2 measurement is shown on the right. Spectra shown are medians of twelve 5-s scans, with modulation amplitude set independently to 1/3 of the narrowest observed linewidth, scan range equal to $10 \times$ the full-width half-maximum linewidth, and other acquisition parameters held constant. Signal-to-noise ratios are 43 and 103, respectively, reflective of the differences in linewidth

Table 1 Initial pO_2 measurements for IR sensors in the brain and hind leg

Rabbit ID (cohort)	Measurement date	Intra-cranial pO_2 (mmHg, mean ± SD)		Hind leg pO_2 (mmHg, mean ± SD)	
		Sensor 1	Sensor 2	Sensor 1	Sensor 2
9 (3 months)	12/11/2018	58[a]		15 ± 0.2	27 ± 0.9
9 (3 months)	1/4/2019	42 ± 0.6	46 ± 1.1	44 ± 0.2	21 ± 0.3
9 (3 months)	2/19/2019	42 ± 0.8	49 ± 1.4	26 ± 0.5	25 ± 0.1
10 (3 months)	11/14/2018	35	34 ± 0.1	35 ± 4.1	39 ± 2.2
11 (3 months)	12/18/2018	36 ± 0.7	46 ± 1.8	7 ± 0.3	10 ± 0.2
11 (3 months)	1/21/2019	34 ± 0.2	41 ± 0.4	13 ± 0.9	19 ± 0.3
11 (3 months)	2/19/2019	32 ± 0.6	40 ± 0.4	6 ± 0.1	10 ± 0.1
13 (3 months)	12/11/2018	44 ± 0.3	50 ± 0.5	13 ± 1.3	13 ± 1.7
13 (3 months)	1/4/2019	43 ± 0.2	55 ± 0.2	21[a]	
13 (3 months)	2/19/2019	42 ± 1.0	55 ± 3.0	36 ± 3.5	13 ± 4.0
16 (3 months)	12/18/2018	41 ± 4.7	46 ± 8.9	39 ± 0.5	49 ± 1.2
16 (3 months)	1/21/2019	35 ± 1.3	48 ± 2.0	34 ± 0.6	73 ± 1.4
16 (3 months)	2/19/2019	38 ± 0.4	50 ± 0.2	51 ± 2.0	38 ± 1.0
20 (9 months)	1/25/2019	43 ± 4.2	56 ± 7.5	5 ± 0.1	14 ± 0.1
20 (9 months)	5/3/2019	35 ± 0.9	46 ± 2.7	35 ± 1.3	35 ± 1.4
20 (9 months)	8/23/2019	39 ± 0.2[b]		22 ± 3.7[b]	
22 (9 months)	1/25/2019	38 ± 1.1	51 ± 0.7	6 ± 0.8	17 ± 1.5
22 (9 months)	5/3/2019	42 ± 0.7	54 ± 0.4	9 ± 0.3	32 ± 1.0
22 (9 months)	8/23/2019	44 ± 2.6[b]		33 ± 1.5[b]	
23 (9 months)	1/25/2019	47 ± 0.5	50 ± 1.2	c	c
23 (9 months)	5/3/2019	51 ± 0.6	42 ± 0.6	c	c
23 (9 months)	8/23/2019	50 ± 0.6[b]		c	c

[a]Only one component observed: no oxygen reported

[b]No gradient (power supply failure)

[c]No EPR signal detected at this site

3.7 Recalibration of IRs that were Removed Intact from the Tissue

Following removal from the rabbits after euthanasia, functional and calibration studies were repeated. One resonator was recognized as broken during the in vivo phase of the experiment. Another resonator was identified to be broken following removal from the rabbit, but noted to have been fully operational days earlier in vivo. Oximetric calibration of a subset of resonators ($N=4$, two from brain, two from leg) were performed. Resonators were cleaned of any residual tissue remaining following extraction. Average oxygen sensitivity of 7.5 ± 0.4 mG/mmHg and an anoxic linewidth of 112 ± 2 mG were observed. These values are not significantly different from values measured for unimplanted resonators, with sensitivity of 10 ± 1 mG/mmHg ($p=0.09$) and anoxic linewidth of 108 ± 5 mG ($p=0.5$).

Table 2 One-week cohort

	Ref. range	Pre-surgery		Post-surgery	
		IR	Control	IR	Control
WBC	3.1–9.7 10^3/μL	6.475	6	8.1	6.1
Hemoglobin	10.9–14.5 g/dL	12.475	11.525	11.67	10.47
Platelet count	206–705 10^3/μL	222.75	226.75	426.00	369.33
AST (SGOT)	11–36 IU/L	13.5	12.5	15.33	12.33
ALT (SGPT)	22–83 IU/L	25.75	44.5	25.00	31.00
Alk phosphatase	22–119 IU/L	234.5[a]	207.75[a]	118.67	195.67[a]
Creatinine	0.7–1.4 mg/dL	0.9	0.9	0.93	0.77

[a]Measurement beyond reference range

Table 3 Three-month cohort

	Ref. range	Pre surgery		Post surgery	
		IR	Control	IR	Control
WBC	3.1–9.7 10^3/μL	7.85	6.625	7.05	7.5
Hemoglobin	10.9–14.5 g/dL	14.325	13.575	13.65	13.3
Platelet count	206–705 10^3/μL	290.75	260.25	193.25[a]	339.75
AST (SGOT)	11–36 IU/L	13	12.75	17.75	17.25
ALT (SGPT)	22–83 IU/L	31.25	24.75	34.75	28
Alk phosphatase	22–119 IU/L	57	73	33.5	36
Creatinine	0.7–1.4 mg/dL	0.975	1.05	0.925	0.975

[a]Measurement beyond reference range

3.8 Rabbit Laboratory Results

Results were consistent across all cohorts. There were no significant differences in average CBC or CMP profiles between the IR- and HDPE control-implanted rabbits and between labs acquired prior to implantation or prior to sacrifice for any of the three cohorts. All average values were observed to be within the reference range, other than several average alkaline phosphatase levels for both pre-implantation and euthanasia timepoints (138–234 IU/L vs reference range of 22–119 IU/L) and three average platelet counts that were just outside of the lower reference range (Tables 2, 3 and 4). These values are not considered to be clinically significant and may be related to the diet, samples drawn under anesthesia, and/or length of time before samples were spun to separate the serum.

Table 4 Nine-month cohort

	Ref. range	Pre surgery		Post surgery	
		IR	Control	IR	Control
WBC	3.1–9.7 10^3/μL	7.325	7.275	7.3	8.375
Hemoglobin	10.9–14.5 g/dL	13.65	13.625	13.6375	12.725
Platelet count	206–705 10^3/μL	199.25[a]	233	216.125	191.5[a]
AST (SGOT)	11–36 IU/L	12.5	41.5	27	33.5
ALT (SGPT)	22–83 IU/L	18	32.5	25.25	38.5
Alk Phosphatase	22–119 IU/L	151.75[a]	138.25[a]	145[a]	61.25
Creatinine	0.7–1.4 mg/dL	0.775	0.8	0.7875	1

[a]Measurement beyond reference range

3.9 Rabbit Gross Pathology Results

Gross pathology at the 1-week endpoint appeared normal with the exception of naturally healing surgical wounds related to placement of the IRs and control implants in the brain and leg tissues. In these instances, for both the IRs and HDPE controls, the tissue in the region underneath the skin incision revealed healing tissue and in the case of the brain implant a burr hole through the skull. Gross pathology at the 3-month endpoint appeared similar to that at week 1, with the exception of a thin layer of fibrosis surrounding the implant. For the 9-month cohort, gross pathology again appeared similar to that at the 1-week timepoint, with the observation of a thicker layer of fibrosis surrounding the IRs in subcutaneous tissue. Other organs including liver, kidneys, lymph nodes, spinal cord, heart, lungs, stomach and intestines appeared grossly normal.

3.10 Animals Euthanized Early Related to Procedural Complications

Three rabbits with control implants were euthanized on post-implantation days 1–6. Two of them sustained brain injuries secondary to migration of one implant into the optic canal and immediate post-implantation hemorrhage with another implant, both causing neurological injury. For both of these rabbits, the control implants on the right hind leg were inside of muscle as expected with no evidence of bleeding in the surrounding tissue. One of the control rabbits sustained injury from the leg implant resulting in inability to use the right leg. Imaging (MRI—9.4 T Bruker) suggested that the IR penetrated the sciatic nerve. Upon removal, the control implant was found to be deep inside of muscle with no evidence of excessive bleeding in surrounding tissue. Further dissection confirmed the imaging result.

One rabbit with the IR required early euthanasia on post implantation day 2 due to a significant head tilt to the left. Imaging (Fluoroscopy OEC 9800) indicated that the brain IR was reoriented 180° from an anterior to a posterior position. Surgical wounds were present as expected. Tissues underneath the skin incision over the

skull exhibited mild hemorrhage. The IR was in the burr hole on skull in a reversed position, relative to orientation established during implantation, with the IR present in the brain tissue.

3.11 Rabbit Histopathology Results

H+E staining was performed on tissue specimens adjacent to the IRs and HDPE controls implanted in the rabbit hind leg for all 3 cohorts. After both 1-week and 3-month implantations, the levels of inflammatory reactions were consistent with expected implantation trauma and similar in both IR and control implantations. No leakage of LiNc-BuO crystals was found in any of the tracks or surrounding muscle tissues for any samples (Fig. 7). For the 9-month cohort of rabbits, fibrosis was again observed both in control and IR samples in the tissue surrounding the transmission line as well as the coupling loop on H+E staining (Fig. 8). No hemorrhage or leakage of the LiNc-BuO crystals was observed in the experimental group.
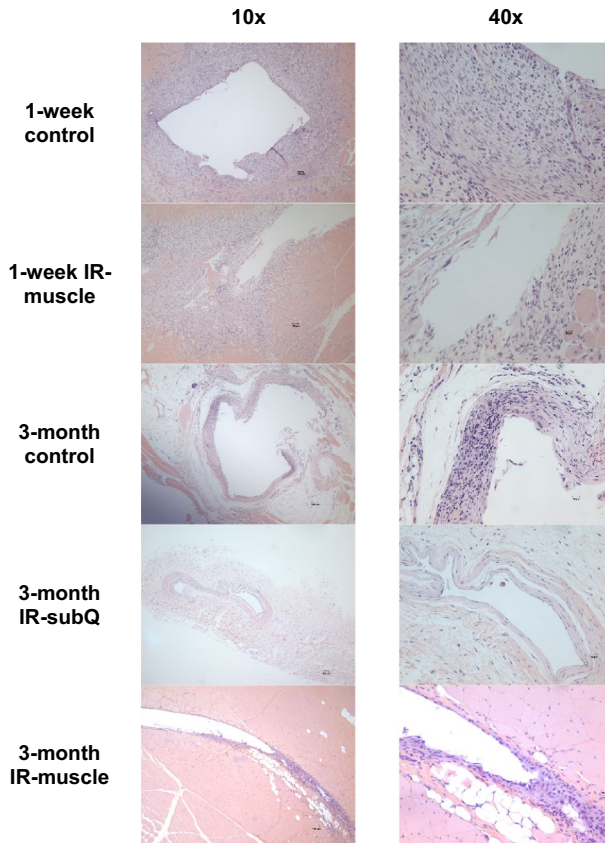
Fig. 7 H+E staining images obtained from tissue specimens adjacent to the IR and HDPE control implanted in the rabbit hind leg (shown at 10× and 40× magnifications)
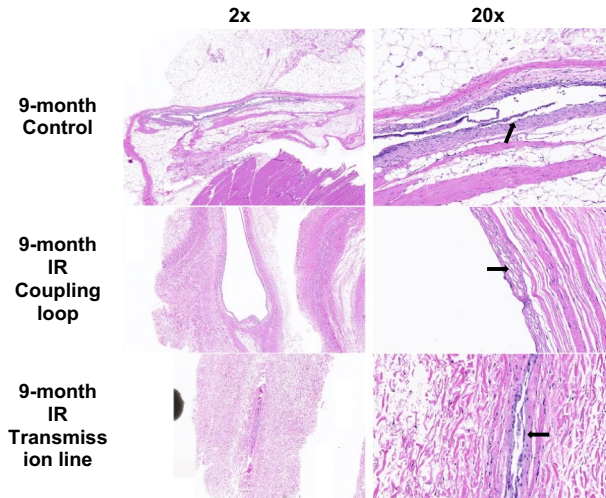
Fig. 8 H+E staining images obtained from tissue specimens adjacent to the IR and HDPE control implanted in the rabbit hind leg (shown at 2× and 20× magnifications). At 9-month post-implantation, there is minor inflammation and foreign body reaction. Fibrosis was observed both in the control and the IR in the tissue surrounding the transmission line as well as the coupling loop (short arrows). No hemorrhage or leakage of the LiNc-BuO crystals was observed in the experimental group

4 Discussion

The refinements to the IR design including the second biocompatible PTFE coating over the LiNc-BuO and PDMS along the transmission line, the circular disk to maintain the shape of the coupling loop, and the peel-away catheter for implantation showed safety, oximetry capability, and implementability of EPR oximetry in deep tissues. Biocompatibility tests demonstrated reactions within the normal expected range. The rabbit study confirmed that the IR can be safely implanted into brain and leg tissues and that oxygen measurements in deep tissue could be obtained repeatedly using EPR oximetry. The IR did not cause any more tissue reaction around the implant than the control HDPE implant.

In the preclinical rabbit study, we identified a mechanical failure at the intersection of the twisted pair of the transmission line and the coupling loop of the IR. Breakage of one or both wires of the twisted pair transmission line occurred in 2 resonators implanted for 9 months in the hind leg of the rabbit, though one break is expected to have occurred during explantation. Assuming that the physiological motion of the implantable resonator in the leg tissue created work hardening of the metal wire at this junction, we have designed, machined, and tested a new injection mold prototype to incorporate extra PDMS around this juncture to provide additional strain relief at this critical point. The breakage that occurred during explantation might have resulted from fibrosis surrounding the IR, making removal of the IR challenging. The coupling loop may benefit from secondary PTFE encapsulation similar to the transmission line.

The latest refinements of the IR for EPR oximetry in deep tissues have been made with the intention to easily translate this technology into clinical practice. The currently available oxygen probes for clinical EPR oximetry include India ink and Oxy-Chip [26, 27]. Both Inda ink and OxyChip have been implanted during a minimally invasive clinic procedure with or without a local anesthetic prior to their surgical, radiation, or chemotherapy treatments. Non-invasive EPR oximetry was able to be performed at multiple timepoints during some of the patient's treatment course. The IR implantation procedure using the brachytherapy needle and peel-away catheter that was outlined in the rabbit study can be easily translated to human patients. The brachytherapy needles and peel-away catheters (during central venous catheter placement) are routinely used in clinical practice. Initially, the implantation procedure may need to be done under sedation depending on the site of implantation. The skin incision required to bury the coupling loop is small (1.0–1.5 cm), so the IR implantation in non-brain sites would be considered a minor procedure from a surgical point of view.

5 Conclusions

The revised version of the IR comprised of LiNc-BuO crystals in PDMS with a second biocompatible PTFE coating over the PDMS-coated MP35N transmission lines and the circular disk to maintain the shape of the coupling loop exhibited stability and biocompatibility. The IR was tolerated in the rabbit's brain and leg for up to 9 months after implantation and provided tissue oxygen measurements using EPR oximetry. The tissue surrounding the implantable resonator showed no more tissue reaction than the tissues surrounding the control implants. This pre-clinical study in rabbits establishes that the IR can be safely implanted in the brain and leg tissue and can provide repeated, non-invasive EPR oxygen measurements in vivo.

Declarations

References

1. S. Rockwell, I. Dobrucki, E. Kim, S. Marrison, V. Vu, Hypoxia and radiation therapy: past history, ongoing research, and future promise. Curr Mol Med **9**, 442–458 (2009). https://doi.org/10.2174/156652409788167087

2. B.S. Sørensen, M.R. Horsman, Tumor hypoxia: impact on radiation therapy and molecular pathways. Front Oncol **10**, 562 (2020)

3. M.R. Horsman, J. Overgaard, The impact of hypoxia and its modification of the outcome of radiotherapy. J Radiat Res **57**(S1), i90–i98 (2016)

4. J.M. Brown, The hypoxic cell: a target for selective cancer therapy—eighteenth Bruce F. Cain Memorial Award lecture. Cancer Res. **59**(23), 5863–5870 (1999)

5. D.M. Brizel, G.S. Sibley, L.R. Prosnitz, R.L. Scher, M.W. Dewhirst, Tumor hypoxia adversely affects the prognosis of carcinoma of the head and neck. Int J Radiat Oncol Biol Phys **38**, 285–289 (1997). https://doi.org/10.1016/S0360-3016(97)00101-6

6. P. Vaupel, Hypoxia and aggressive tumor phenotype: implications for therapy and prognosis. Oncologist **13**(Suppl 3), 21–26 (2008). https://doi.org/10.1634/theoncologist.13-S3-21;10.1634/theoncologist.13-S3-21

7. M. Höckel, K. Schlenger, B. Aral, M. Mitze, U. Schäffer, P. Vaupel, Association between tumor hypoxia and malignant progression in advanced cancer of the uterine cervix. Cancer Res **56**, 4509–4515 (1996)

8. K. Begg, M. Tavassoli, Inside the hypoxic tumour: reprogramming of the DDR and radioresistance. Cell Death Discov. **6**, 1234567890 (2020)

9. T.G. Graeber, C. Osmanian, T. Jacks, D.E. Housman, C.J. Koch, S.W. Lowe, A.J. Giaccia, Hypoxia-mediated selection of cells with diminished apoptotic potential in solid tumours. Nature **379**, 88–91 (1996). https://doi.org/10.1038/379088a0

10. H.M. Swartz, A.B. Flood, P.E. Schaner, H. Howard, B.B. Williams, B.W. Pogue, B. Gallez, How best to interpret measures of levels of oxygen in tissues to make them effective clinical tools for care of patients with cancer and other oxygen-dependent pathologies. Physiol Rep **8**, 14541 (2020)

11. H.M. Swartz, A.B. Flood, B.B. Williams, B.W. Pogue, P.E. Schaner, P. Vaupel, What is the meaning of an oxygen measurement? in *Oxygen Transport to Tissue XLII. Advances in Experimental Medicine and Biology*, vol. 1269, ed. by E.M. Nemoto, E.M. Harrison, S.C. Pias, D.E. Bragin, D.K. Harrison, J.C. LaManna (Springer, Cham, 2021). https://doi.org/10.1007/978-3-030-48238-1_48

12. W.R. Wilson, M.P. Hay, Targeting hypoxia in cancer therapy. Nat Rev Cancer **11**, 393–410 (2011)

13. V.L. Codony, M. Tavassoli, Hypoxia-induced therapy resistance: available hypoxia-targeting strategies and current advances in head and neck cancer. Transl Oncol **14**, 101017 (2021). https://doi.org/10.1016/j.tranon.2021.101017

14. K. Pinker, P. Andrzejewski, P. Baltzer, S.H. Polanec, A. Sturdza, D. Georg, T.H. Helbich, G. Karanikas, C. Grimm, S. Polterauer, R. Poetter, W. Wadsak, M. Mitterhauser, P. Georg, Multiparametric [18F]fluorodeoxyglucose/[18F]fluoromisonidazole positron emission tomography/ magnetic resonance imaging of locally advanced cervical cancer for the non-invasive detection of tumor heterogeneity: a pilot study. PLoS ONE (2016). https://doi.org/10.1371/journal.pone.0155333

15. Z. Xu, X.F. Li, H. Zou, X. Sun, B. Shen, 18F-Fluoromisonidazole in tumor hypoxia imaging. Oncotarget **8**(55), 94969 (2017)

16. J.P.B. O'Connor, S.P. Robinson, J.C. Waterton, Imaging tumour hypoxia with oxygen-enhanced MRI and BOLD MRI. Br J Radiol (2019). https://doi.org/10.1259/bjr.20180642

17. J.V. Gaustad, A. Hauge, C.S. Wegner, T.G. Simonsen, K.V. Lund, L.M.K. Hansem, E.K. Rofstad, DCE-MRI of tumor hypoxia and hypoxia-associated aggressiveness. Cancers (Basel) **12**, 1–14 (2020). https://doi.org/10.3390/cancers12071979

18. H. Lyng, K. Sundfør, E.K. Rofstad, Oxygen tension in human tumours measured with polarographic needle electrodes and its relationship to vascular density, necrosis and hypoxia. Radiother Oncol **44**, 163–169 (1997). https://doi.org/10.1016/S0167-8140(97)01920-8

19. M. Nordsmark, S.M. Bentzen, J. Overgaard, Measurement of human tumour oxygenation status by a polarographic needle electrode: an analysis of inter- and intratumour heterogeneity. Acta Oncol (Madr) **33**, 383–389 (1994). https://doi.org/10.3109/02841869409098433

20. M. Höckel, C. Knoop, K. Schlenger, B. Vorndran, E. Baußmann, M. Mitze, P.G. Knapstein, P. Vaupel, Intratumoral pO_2 predicts survival in advanced cancer of the uterine cervix. Radiother Oncol **26**, 45–50 (1993). https://doi.org/10.1016/0167-8140(93)90025-4

21. N. Khan, H. Hou, S. Hodge, M. Kuppusamy, E.Y. Chen, A. Eastman, P. Kuppusamy, H.M. Swartz, Recurrent low-dose chemotherapy to inhibit and oxygenate head and neck tumors, in *Oxygen transport to tissue XXXVI*. ed. by H.M. Swartz, D.K. Harrison, D.F. Bruley (Springer, New York, 2014), pp. 105–111

22. N. Khan, H. Hou, C.J. Eskey, K. Moodie, S. Gohain, G. Du, S. Hodge, W.C. Culp, P. Kuppusamy, H.M. Swartz, Deep-tissue oxygen monitoring in the brain of rabbits for stroke research. Stroke **46**, e62–e66 (2015). https://doi.org/10.1161/STROKEAHA.114.007324

23. H. Hou, O. Grinberg, B. Williams, S. Grinberg, H. Yu, D.L. Alvarenga, H. Wallach, J. Buckey, H.M. Swartz, The effect of oxygen therapy on brain damage and cerebral pO_2 in transient focal cerebral ischemia in the rat. Physiol Meas **28**, 963–976 (2007). https://doi.org/10.1088/0967-3334/28/8/017

24. M.A. Polacco, H. Hou, P. Kuppusamy, E.Y. Chen, Measuring flap oxygen using electron paramagnetic resonance oximetry. Laryngoscope **129**, E415–E419 (2019). https://doi.org/10.1002/lary.28043

25. H. Hou, S.P. Mupparaju, J.P. Lariviere, S. Hodge, J. Gui, H.M. Swartz, N. Khan, Assessment of the changes in 9L and C6 glioma pO_2 by EPR oximetry as a prognostic indicator of differential response to radiotherapy. Radiat Res **179**, 343–351 (2013). https://doi.org/10.1667/RR2811.1;10.1667/RR2811.1

26. A.B. Flood, V.A. Wood, H.M. Swartz, Using India ink as a sensor for oximetry: evidence of its safety as a medical device, in *Oxygen transport to tissue XXXIX*. ed. by H.J. Halpern, J.C. LaManna, D.K. Harrison, B. Epel (Springer International Publishing, Cham, 2017), pp. 297–312

27. P.E. Schaner, J.R. Pettus, A.B. Flood, B.B. Williams, L.A. Jarvis, E.Y. Chen, D.A. Pastel, R.A. Zuurbier, R.M. DiFlorio-Alexander, H.M. Swartz, P. Kuppusamy, OxyChip implantation and subsequent electron paramagnetic resonance oximetry in human tumors is safe and feasible: first experience in 24 patients. Front Oncol (2020). https://doi.org/10.3389/fonc.2020.572060

28. H.M. Swartz, B.B. Williams, H. Hou, N. Khan, L.A. Jarvis, E.Y. Chen, P.E. Schaner, A. Ali, B. Gallez, P. Kuppusamy, A.B. Flood, Direct and repeated clinical measurements of pO_2 for enhancing cancer therapy and other applications, in *Oxygen transport to tissue XXXVIII*. ed. by Q. Luo, L.Z. Li, D.K. Harrison, H. Shi, D.F. Bruley (Springer, Cham, 2016), pp. 95–104

29. G. Meenakshisundaram, E. Eteshola, R.P. Pandian, A. Bratasz, S.C. Lee, P. Kuppusamy, Fabrication and physical evaluation of a polymer-encapsulated paramagnetic probe for biomedical oximetry. Biomed Microdevices **11**, 773–782 (2009). https://doi.org/10.1007/s10544-009-9292-x

30. G. Meenakshisundaram, R.P. Pandian, E. Eteshola, S.C. Lee, P. Kuppusamy, A paramagnetic implant containing lithium naphthalocyanine microcrystals for high-resolution biological oximetry. J Magn Reson **203**, 185–189 (2010). https://doi.org/10.1016/j.jmr.2009.11.016

31. H. Hou, N. Khan, M. Nagane, S. Gohain, E.Y. Chen, L.A. Jarvis, P.E. Schaner, B.B. Williams, A.B. Flood, H.M. Swartz, P. Kuppusamy, Skeletal muscle oxygenation measured by EPR oximetry using a highly sensitive polymer-encapsulated paramagnetic sensor, in *Oxygen transport to tissue XXXVIII*. ed. by Q. Luo, L.Z. Li, D.K. Harrison, H. Shi, D.F. Bruley (Springer, Cham, 2016), pp. 351–357

32. Sergey Petryakov, Wilson Schreiber, Maciej Kmiec, Harold M. Swartz, Philip E. Schaner, Benjamin Williams (2021) Flexible, segmented surface coil resonator for in vivo EPR oximetry. Appl Magn Reson (special issue)

33. H.J. Halpern, D.P. Spencer, J. Van Polen, M.K. Bowman, A.C. Nelson, E.M. Dowey, B.A. Teicher, Imaging radio frequency electron-spin-resonance spectrometer with high resolution and sensitivity for in vivo measurements. Rev Sci Instrum **60**, 1040–1050 (1989). https://doi.org/10.1063/1.1140314

34. Y. Deng, G. He, S. Petryakov, P. Kuppusamy, J.L. Zweier, Fast EPR imaging at 300 MHz using spinning magnetic field gradients. J Magn Reson **168**, 220–227 (2004). https://doi.org/10.1016/j.jmr.2004.02.012

35. G.A. Rinard, R.W. Quine, S.S. Eaton, G.R. Eaton, Frequency dependence of EPR signal intensity, 250 MHz to 9.1 GHz. J Magn Reson **156**, 113–121 (2002). https://doi.org/10.1006/jmre.2002.2530

36. S. Subramanian, K.I. Matsumoto, J.B. Mitchell, M.C. Krishna, Radio frequency continuous-wave and time-domain EPR imaging and Overhauser-enhanced magnetic resonance imaging of small animals: Instrumental developments and comparison of relative merits for functional imaging. NMR Biomed. **17**, 263–294 (2004)

37. B. Epel, S.V. Sundramoorthy, E.D. Barth, C. Mailer, H.J. Halpern, Comparison of 250 MHz electron spin echo and continuous wave oxygen EPR imaging methods for in vivo applications. Med Phys **38**, 2045–2052 (2011). https://doi.org/10.1118/1.3555297

38. B. Epel, S.V. Sundramoorthy, C. Mailer, H.J. Halpern, A versatile high speed 250-MHz pulse imager for biomedical applications. Concepts Magn Reson Part B Magn Reson Eng **33**, 163–176 (2008). https://doi.org/10.1002/cmr.b.20119

39. H. Hirata, S. Petryakov, W. Schreiber, Resonators for clinical electron paramagnetic resonance (EPR), in *measuring oxidants and oxidative stress in biological system*. ed. by L. Berliner, N. Parinandi (Springer, Cham, 2020), pp. 189–219

40. S. Petryakov, A. Samouilov, M. Chzhan-Roytenberg, E. Kesselring, Z. Sun, J.L. Zweier, Segmented surface coil resonator for in vivo EPR applications at 1.1 GHz. J Magn Reson **198**, 8–14 (2009). https://doi.org/10.1016/j.jmr.2008.12.014

41. H. Li, H. Hou, A. Sucheta, B. Williams, J. Lariviere, M. Khan, P. Lesniewski, B. Gallez, H. Swartz, Implantable resonators-a technique for repeated measurement of oxygen at multiple deep sites with in vivo EPR, in *Oxygen transport to tissue XXXI*. (Springer, Boston, 2010), pp. 265–272

42. R.M. Caston, W. Schreiber, H. Hou, B.B. Williams, E.Y. Chen, P.E. Schaner, L.A. Jarvis, A.B. Flood, S.V. Petryakov, M.M. Kmiec, P. Kuppusamy, H.M. Swartz, Development of the implantable resonator system for clinical EPR oximetry. Cell Biochem Biophys **75**, 275–283 (2017). https://doi.org/10.1007/s12013-017-0809-2

43. H. Hou, R. Dong, H. Li, B. Williams, J.P. Lariviere, S.K. Hekmatyar, R.A. Kauppinen, N. Khan, H. Swartz, Dynamic changes in oxygenation of intracranial tumor and contralateral brain during tumor growth and carbogen breathing: a multisite EPR oximetry with implantable resonators. J Magn Reson **214**, 22–28 (2012). https://doi.org/10.1016/j.jmr.2011.09.043

44. H. Hou, H. Li, R. Dong, S. Mupparaju, N. Khan, H. Swartz, Cerebral oxygenation of the cortex and striatum following normobaric hyperoxia and mild hypoxia in rats by EPR oximetry using multi-probe implantable resonators, in *Oxygen transport to tissue XXXII*. ed. by J.C. LaManna, M.A. Puchowicz, K. Xu, D.K. Harrison, D.F. Bruley (Springer, Boston, 2011), pp. 61–67

45. H. Hou, N. Khan, J. Lariviere, S. Hodge, E.Y. Chen, L.A. Jarvis, A. Eastman, B.B. Williams, P. Kuppusamy, H.M. Swartz, Skeletal muscle and glioma oxygenation by carbogen inhalation in rats: a longitudinal study by EPR oximetry using single-probe implantable oxygen sensors, in *Oxygen transport to tissue XXXVI*. ed. by H.M. Swartz, D.K. Harrison, D.F. Bruley (Springer, New York, 2014), pp. 97–103

46. H.M. Swartz, R.B. Clarkson, The measurement of oxygen in vivo using EPR techniques. Phys Med Biol **43**, 1957–1975 (1998)

47. N. Khan, B.B. Williams, H. Hou, H. Li, H.M. Swartz, Repetitive tissue pO_2 measurements by electron paramagnetic resonance oximetry: current status and future potential for experimental and clinical studies. Antioxid Redox Signal **9**, 1169–1182 (2007). https://doi.org/10.1089/ars.2007.1635

48. H.M. Swartz, S. Boyer, P. Gast, J.F. Glockner, H. Hu, K.J. Liu, M. Moussavi, S.W. Norby, N. Vahidi, T. Walczak, M. Wu, R.B. Clarkson, Measurements of pertinent concentrations of oxygen in vivo. Magn Reson Med **20**, 333–339 (1991). https://doi.org/10.1002/mrm.1910200217

49. H.M. Swartz, T. Walczak, Developing in vivo EPR oximetry for clinical use, in *Oxygen transport to tissue XX*. ed. by A.G. Hudetz, D.F. Bruley (Springer, Boston, 1998), pp. 243–252

50. H. Hou, N. Khan, S. Gohain, C.J. Eskey, K.L. Moodie, K.J. Maurer, H.M. Swartz, P. Kuppusamy, Dynamic EPR oximetry of changes in intracerebral oxygen tension during induced thromboembolism. Cell Biochem Biophys **75**, 285–294 (2017). https://doi.org/10.1007/s12013-017-0798-1

51. Schreiber W, Petryakov S V., Kmiec MM, Flood AB, Swartz HM, Schaner PE, Williams. BB (2021) In vivo cw-epr spectrometer systems for dosimetry and oximetry in preclinical and clinical applications. Appl Magn Reson (special issue)

52. O.Y. Grinberg, H. Hou, S.A. Grinberg, K.L. Moodie, E. Demidenko, B.J. Friedman, M.J. Post, H.M. Swartz, pO_2 and regional blood flow in a rabbit model of limb ischemia. Physiol Meas **25**(3), 659 (2004)

Publisher's Note Springer Nature remains neutral with regard to jurisdictional claims in published maps and institutional affiliations.

Authors and Affiliations

Eunice Y. Chen[1,2] · Dan Tse[2,3] · Huagang Hou[2,3] · Wilson A. Schreiber[2,3] · Philip E. Schaner[2,4] · Maciej M. Kmiec[2,3] · Kendra A. Hebert[2,3] · Periannan Kuppusamy[2,3] · Harold M. Swartz[2,3,4] · Benjamin B. Williams[2,3,4]

[1]   Section of Otolaryngology, Department of Surgery, Dartmouth-Hitchcock Medical Center, Lebanon, NH, USA

[2]   Geisel School of Medicine at Dartmouth, Hanover, NH, USA

[3]   Department of Radiology, Geisel School of Medicine at Dartmouth, Hanover, NH, USA

[4]   Section of Radiation Oncology, Department of Medicine, Dartmouth-Hitchcock Medical Center, 1 Medical Center Drive, Lebanon, NH 03756, USA